Design of Segmental Bridges for Thermal Gradient

Kenneth W. Shushkewich
Ph.D., P.E.
Project Manager
T.Y. Lin International
San Francisco, California

Thermocouple data from an instrumented prestressed concrete segmental bridge (North Halawa Valley Viaduct) have been efficiently reduced graphically to determine the critical positive and negative thermal gradient. The results are compared with those recommended by various AASHTO specifications. A simplification to the computation procedure for the analysis of segmental bridges for nonlinear thermal gradient is proposed. A fully worked numerical design example is included to demonstrate how the analysis is greatly simplified, and to discuss the impact of the design thermal gradient on the prestressing requirements.

This article presents a state-of-the-art paper on practical segmental bridge design for thermal gradient. The evolution of the design positive and negative thermal gradient in North America over the past 20 years is described. The recommendations given by three current AASHTO specifications are reviewed and compared. The prestressed concrete segmental bridge shown in Fig. 1 (North Halawa Valley Viaduct in Hawaii) has been extensively instrumented with thermocouples at a midspan section and a pier section, and readings are being taken over a five-year period (1995-1999).

The processing of thermocouple readings to-date reveals that the results correlate extremely well with the positive and negative thermal gradients in a proposed revision to an AASHTO specification. These results are particularly timely because they validate the proposed reduction of the negative thermal gradient by 40 percent and substantiate the use of the positive thermal gradient. The general analysis of a segmental bridge for thermal gradient is discussed, and a simplification to the computation procedure is introduced.

A detailed numerical design example (North Halawa Valley Viaduct) is included to demonstrate how the analysis is greatly simplified, and to discuss the impact of thermal gradient on prestressing requirements. Because thermal gradients act on all completed segmental bridges in a similar manner, it should be emphasized that the method advocated in this paper applies equally to precast and cast-in-place

Fig. 1. North Halawa Valley Viaduct.

segmental bridges built by a variety of construction methods (including balanced cantilever, span-by-span, incremental launch, and others).

BACKGROUND

The first breakthrough in the design of segmental bridges for thermal gradient came when the recommendations of the PCI-PTI (Prestressed Concrete Institute-Post-Tensioning Institute)[1] and the New Zealand specification[2] became available 20 years ago. The PCI-PTI suggested a constant gradient over the top slab with a temperature differential of 18°F (10°C). The New Zealand specification considered a fifth order parabola over a depth of 47.2 in. (1200 mm) with a temperature differential of 57.6°F (32°C).

Hoffman, McClure and West[3] conducted a thermal study on an experimental segmental bridge in Pennsylvania. They found that the stresses predicted by the New Zealand specification compared favorably with the experimental results. They also found that the stress at the bottom of the section could be made to agree with the experimental results if a temperature differential of 36°F (20°C) were used with the PCI-PTI recommendations instead of the specified 18°F (10°C).

Elbadry and Ghali[4] developed a finite element computer program to determine the nonlinear temperature distribution in concrete bridges and conducted a parametric study to evaluate the effect of various parameters (solar radiation, wind speed, ambient temperature, deck surface cover) on thermal gradient. Cooke, Priestley and Thurston[5] considered the thermal analysis of partially prestressed concrete bridges. Reasonable agreement was found when experimental results were compared to the theory developed to consider the influence of cracking.

Potgieter and Gamble[6] conducted a comprehensive study of nonlinear thermal gradients at various locations in the United States. A finite difference heat flow computer model was developed and the predicted thermal results showed reasonable agreement with experimental measurements taken from a precast concrete segmental bridge (Kishwaukee River Bridge in Illinois). The computer model was then used to compute probable temperature distributions at 26 SOLMET stations across the United States.

Imbsen, Vandershaf, Schamber and Nutt[7] built on the results of Potgieter and Gamble and produced a state-of-the-art report on thermal effects in concrete bridges. This document formed the basis of the AASHTO guide specification on thermal effects in concrete bridges[8] as well as the AASHTO segmental guide specifications.[9] These documents have been the
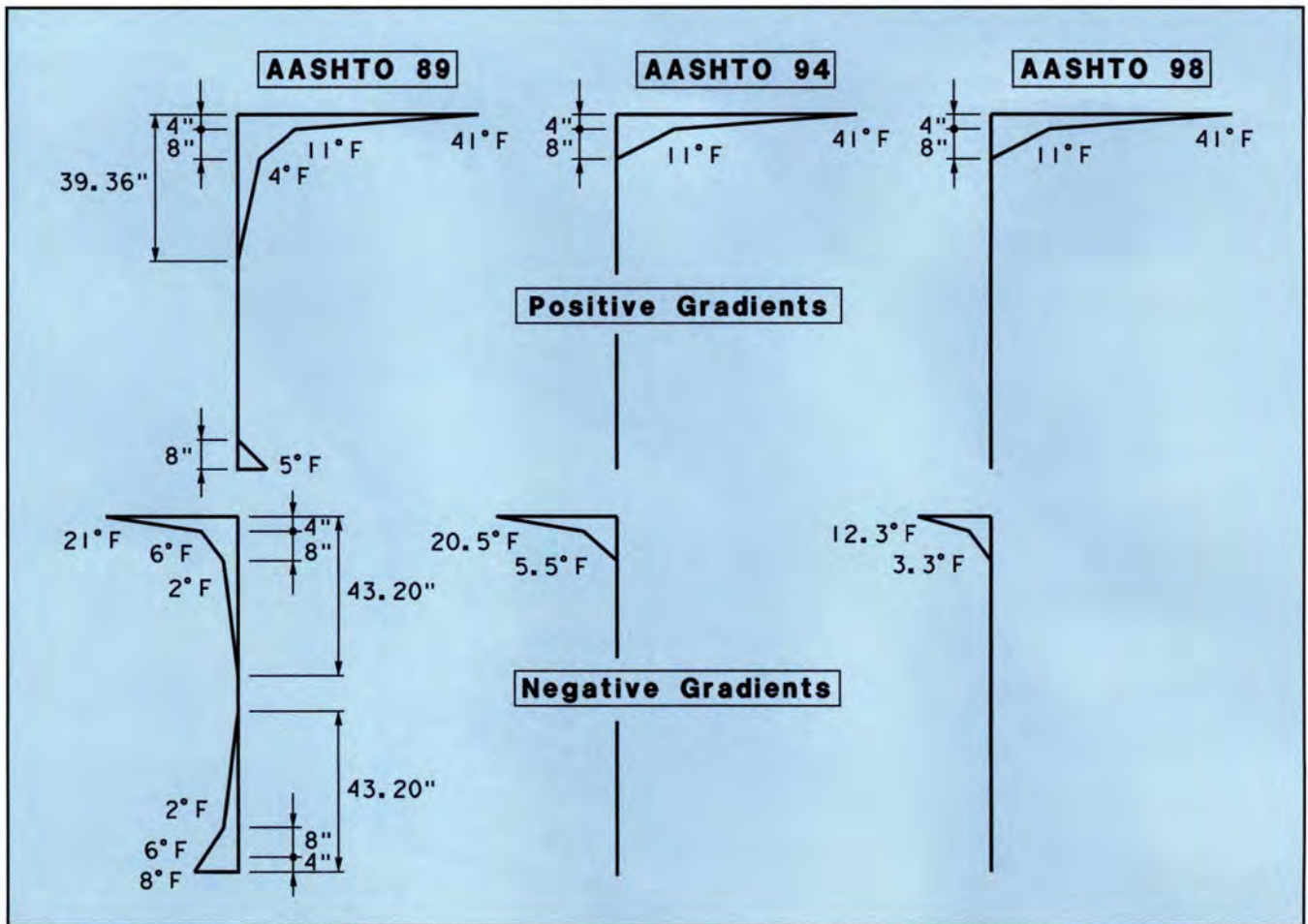
Fig. 2. Comparison of thermal gradients.

basis for the design of segmental bridges for thermal gradient during the past 10 years.

A few refinements have appeared in subsequent specifications. It is interesting to compare the positive and negative thermal gradients (see Fig. 2) in three AASHTO documents (for Zone 3 and plain concrete surface):

1. AASHTO Segmental Guide Specifications[9] (AASHTO 89)

2. AASHTO LRFD Bridge Design Specifications[10] (AASHTO 94)

3. AASHTO proposed Segmental Guide Specifications[11] (AASHTO 98)

The magnitude of the positive gradient is the same for all three gradients [i.e., 41°F, 11°F (22.8°C, 6.1°C)]. The magnitude of the negative gradient is roughly the same for the 89 and 94 gradients [i.e., 21°F, 6°F (11.7°C, 3.3°C)] and reduced by 40 percent for the 98 gradient. Whereas the 89 positive and negative gradients have three pieces at the top and a peak at the bottom, the 94 and 98 gradients have two pieces at the top and no peak at the bottom.

The positive gradient is the same in both the 94 and 98 documents. The negative gradient is -0.50 times the positive gradient in the 94 document, and -0.30 times the positive gradient in the 98 document. Because the results of the instrumentation study validate the 98 gradient, it will be used in the remainder of this paper.

DESCRIPTION OF NORTH HALAWA VALLEY VIADUCT

The North Halawa Valley Viaduct consists of twin prestressed concrete segmental bridges on the island of Oahu in Hawaii (see Fig. 3). The project consists of a 5640 ft (1720 m) inbound viaduct that carries traffic to Honolulu and a 5470 ft (1667 m) outbound viaduct that carries traffic to Kaneohe. The viaducts are on a horizontal curve with a radius of approximately 9500 ft (2900 m), and have a nearly constant grade of 6 percent.

Each viaduct consists of three structural units, with expansion joints at the end of each unit, two fixed piers in the middle of each unit, and expansion piers forming the remainder of the unit. The maximum span length is 360 ft (110 m). The viaduct cross section (see Fig. 4) has a width of 41 ft (12.50 m), which accommodates two lanes of traffic plus shoulders. The depth of the section varies from 18 ft (5.5 m) at the piers to 8 ft (2.4 m) at midspan.

The bridge was designed by T. Y. Lin International of San Francisco, California, in conjunction with Nakamura and Tyau of Honolulu, Hawaii. The bridge design process started in 1988 with the evaluation of seven different alternatives as part of the Major Structures Report. This was followed by the detailed design and construction of the bridge. Kiewit Pacific was awarded the construction contract in early 1992 and given 990 calendar days to complete the project. The bridge (and the entire H-3 Interstate system) opened to traffic in December of 1997.
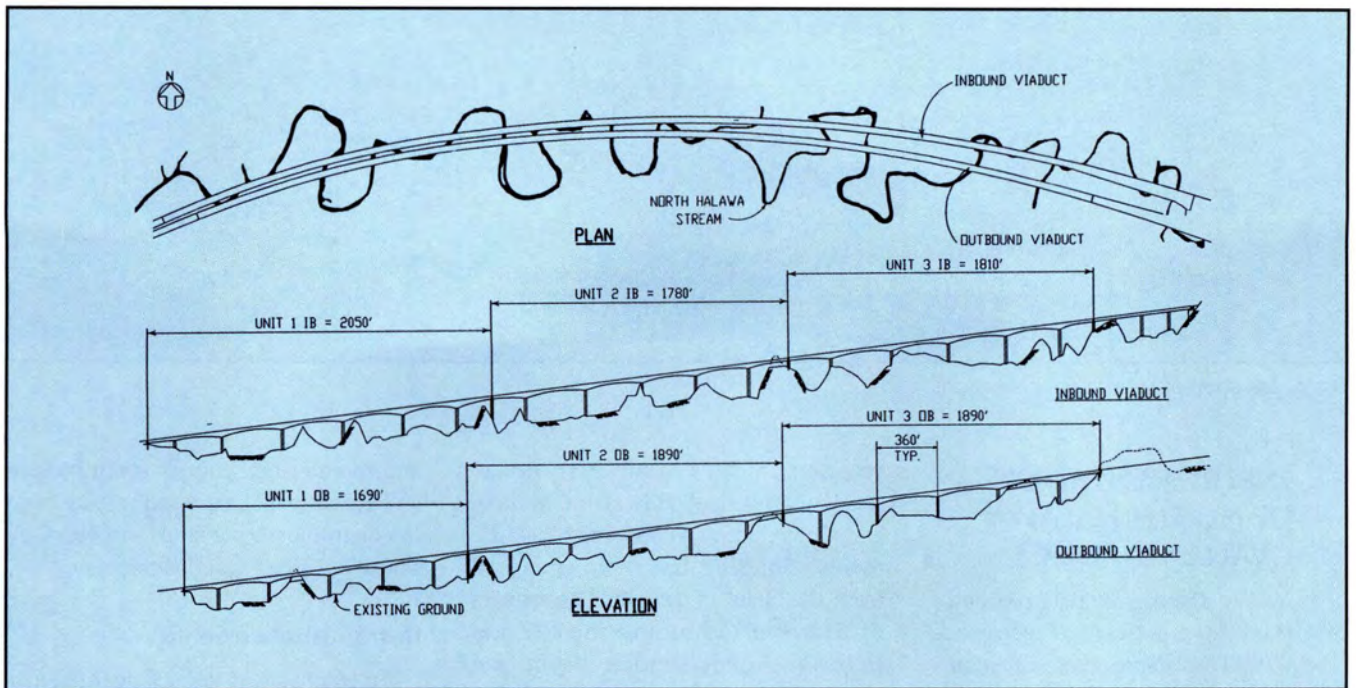
Fig. 3. General plan and elevation of viaduct.

This cast-in-place segmental bridge was built using the balanced cantilever method of construction using form travelers normally associated with cast-in-place segmental construction in combination with launching trusses normally used in precast segmental construction. This project represents the first time in the United States that launching trusses have been used with cast-in-place segmental construction. Additional information on the design and construction of the bridge is given by Ingham, Manzanarez and Cormier.[12]
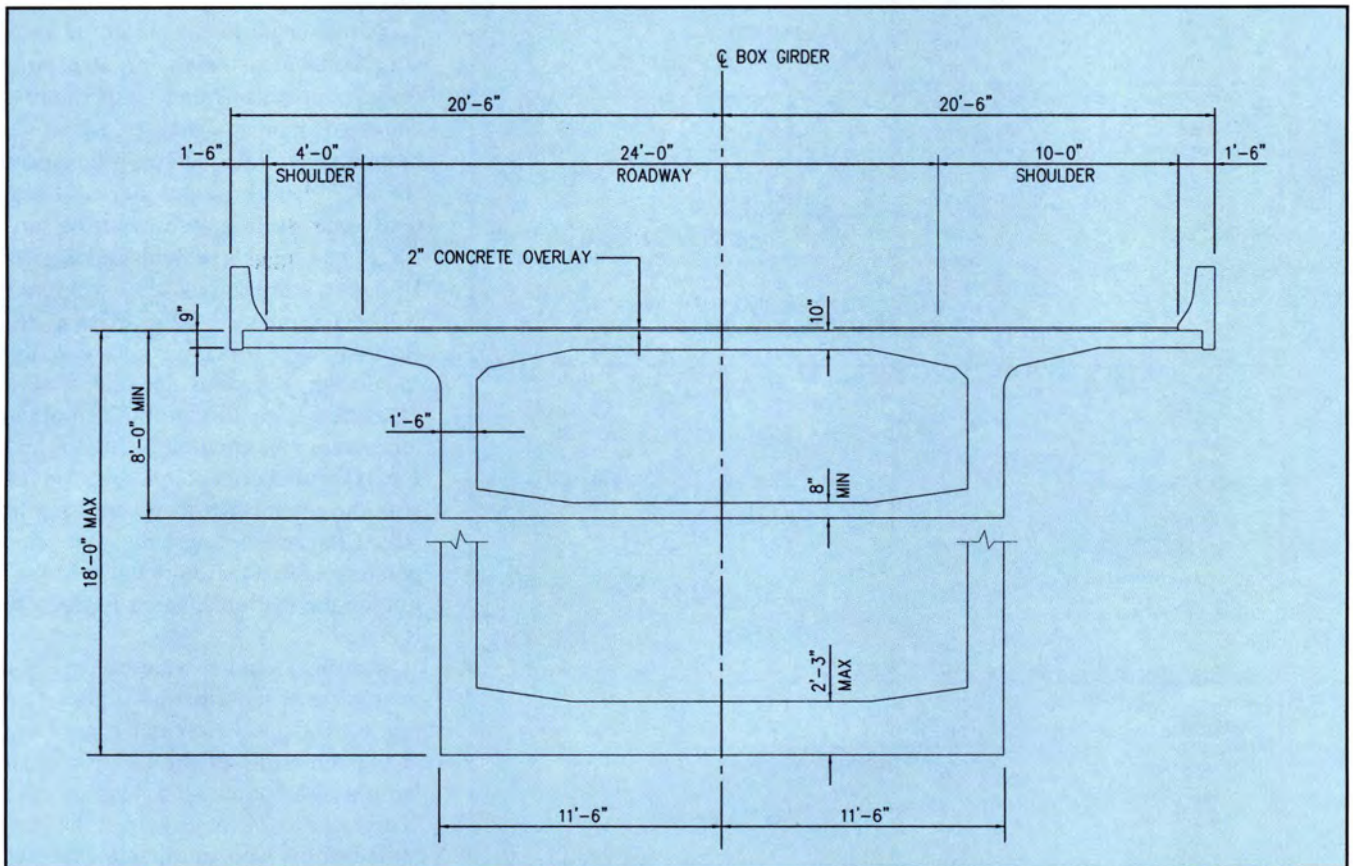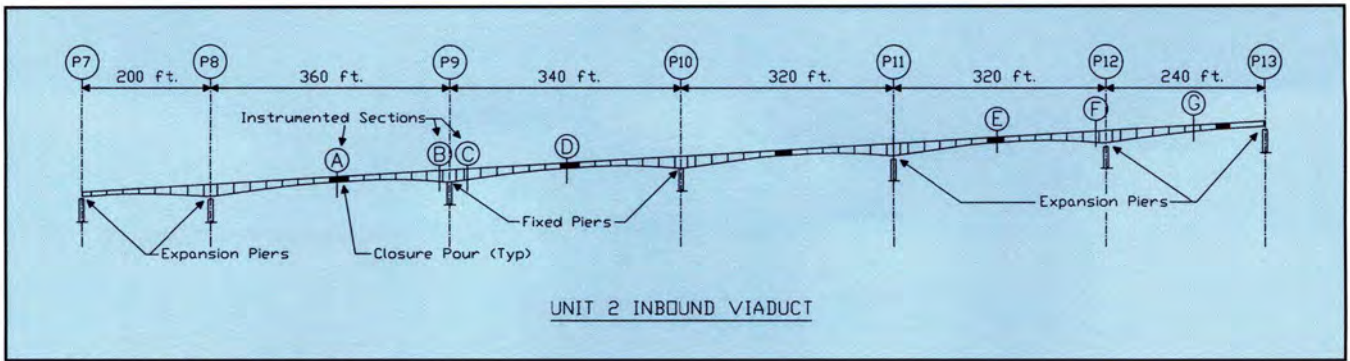

Fig. 4. Bridge cross section.

Fig. 5. Location of instrumented sections.

INSTRUMENTATION OF NORTH HALAWA VALLEY VIADUCT

T. Y. Lin International is presently involved in a five-year program (1995-1999) to instrument and monitor the bridge. The participants in this program are T. Y. Lin International, the University of Hawaii at Manoa, and Construction Technology Laboratories. Funding has been obtained from the State of Hawaii Department of Transportation and the Federal Highway Administration. Additional information on the instrumentation and monitoring setup is given by Lee and Robertson.[13] Detailed results from the instrumentation study are given by Shushkewich, Vo and Robertson.[14]

Instrumentation Setup

An extensive system of instrumentation was set up in Unit 2 Inbound (see Fig. 5). This unit has span lengths of 200, 360, 340, 320, 320 and 240 ft (61, 110, 104, 98, 98 and 73 m). Instrumentation was placed at seven sections. Sections A, D, E and G are termed midspan sections (because they are near midspan), while Sections B, C and F are termed support sections (because they are near supports).

Instrumentation was placed to measure concrete strains, prestressing forces, deflections and temperatures. Concrete strain was measured with vibrating wire strain gauges, mechanical (DEMEC) strain gauges and electrical resistance strain gauges. Prestressing force was measured with load cells. Horizontal deflections were measured with extensometers, while vertical deflections were measured with baseline (piano wire) systems. Rotations were measured with tiltmeters. Temperatures were measured (at Section E and F only) with thermocouples (as well as with the thermistors that were used to adjust the strain gauge data for temperature effects). Additional information on the instrumentation is given in Ref. 13.

Sections E and F were extensively instrumented with thermocouples (see Fig. 6). Gauges 1 to 6 and 7 to 11 are at the centerline of the box girder in the top and bottom slab, respectively. Gauges 12 to 24 (or 26) are at the centerline of the web and monitor the entire depth of the section. Additional
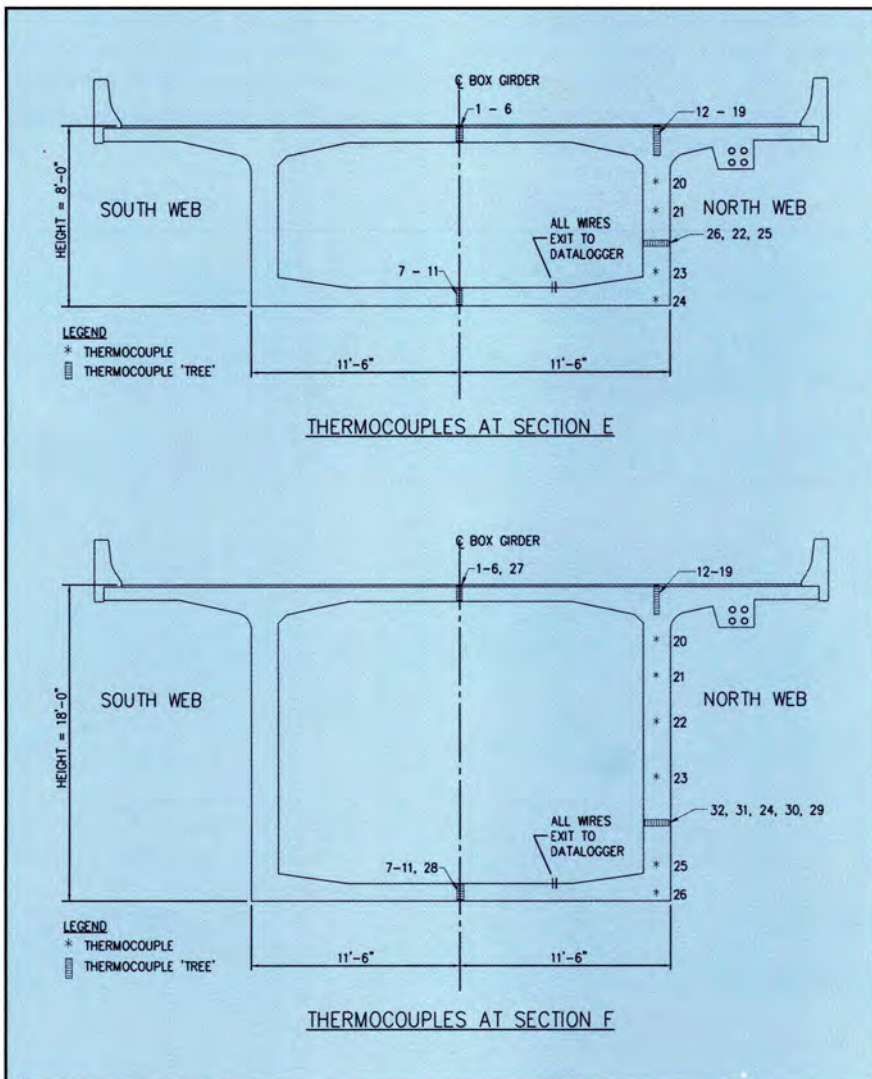

Fig. 6. Thermocouple locations.

1995 Thermocouple Readings at Section E

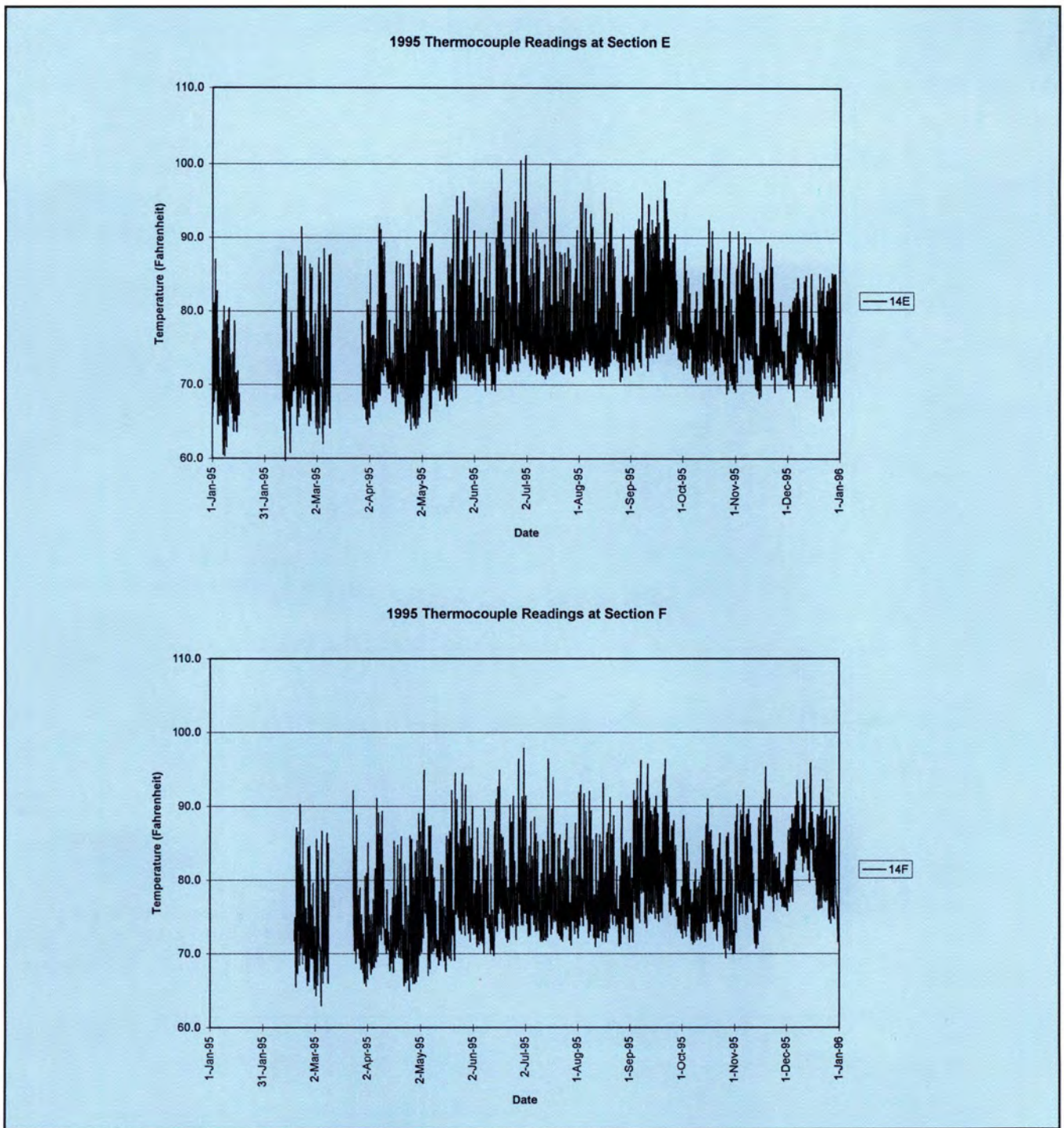**1995 Thermocouple Readings at Section F**

Fig. 7. 1995 thermocouple readings.

gauges are across the width of the web (Gauges 25 and 26 for Section E and Gauges 29 to 32 for Section F).

The thermocouples used in the instrumentation were made using Teflon/Neoflon FEP insulated copper/constantin type-T wire obtained from Omega Measurements. Thermocouple "trees" made of PVC pipe with predrilled holes were used to correctly maintain the location of closely spaced thermocouples during concrete pours.

A reference thermistor provided in the datalogger multiplexer box calibrated the thermocouple readings to record the temperatures directly in degrees Celsius. (Note: °F = 1.8 × °C + 32)

Thermocouple readings were first recorded in late 1994 and will be recorded through the end of 1999. The goal of the thermocouple instrumentation is to obtain critical positive and negative thermal gradients. Readings were taken at 2-hour intervals from

the beginning of the study until August 22, 1995. At this time, it was felt that too much information was being collected (all instrumentation readings were taken at the same 2-hour intervals), and readings were then changed to 6-hour intervals.

It became apparent on October 14, 1997, that the peak critical positive thermal gradient was being underestimated by taking readings at 6-hour intervals so the readings were then
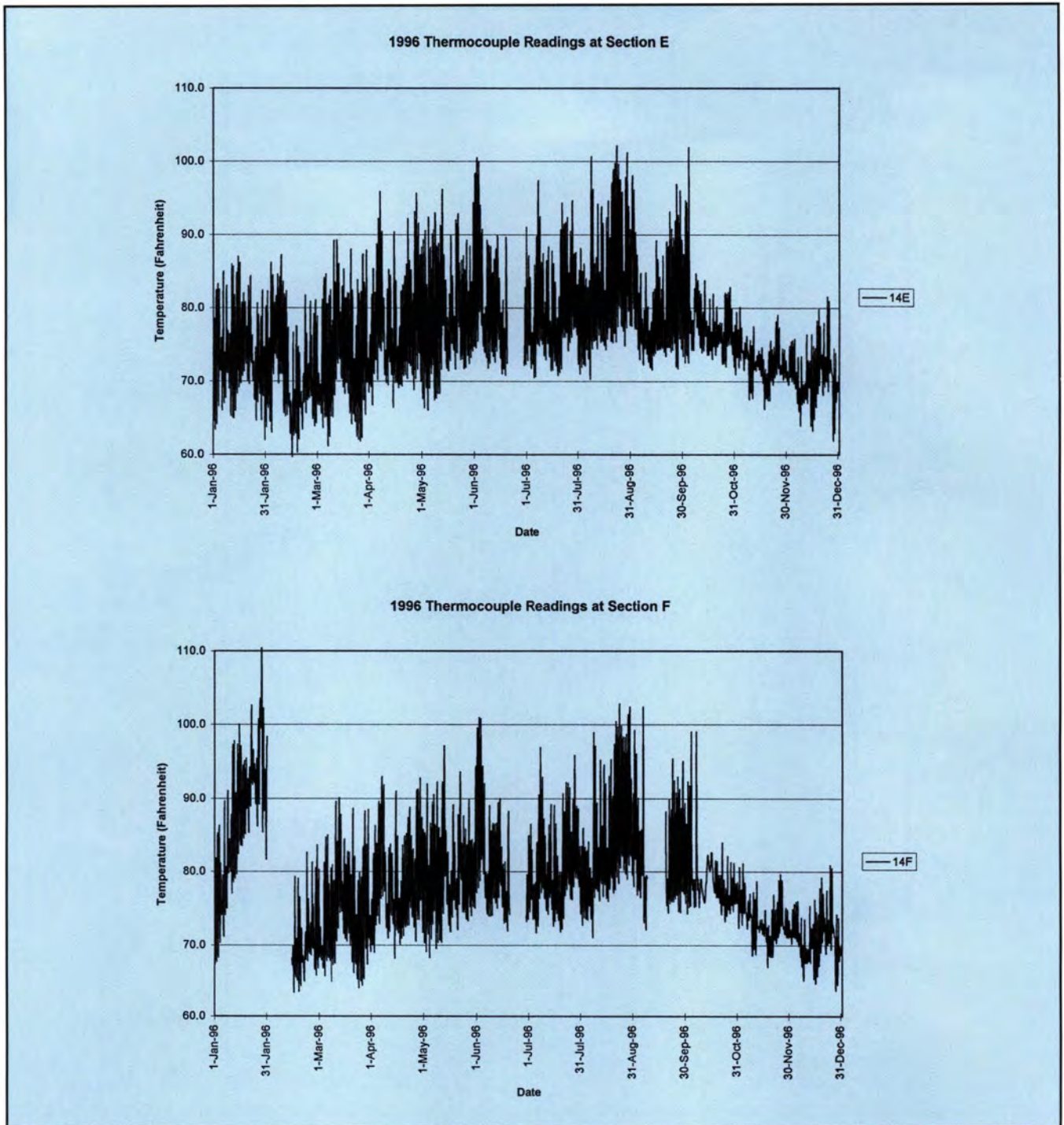
Fig. 8. 1996 thermocouple readings.

changed back to 2-hour intervals for the remainder of the study. Although the positive gradients were underestimated somewhat during the 6-hour interval period, the remainder of the positive gradient readings are informative. Negative gradient readings are not nearly as sensitive to the time interval, so all of the negative gradient readings are useful. The North Halawa Valley Viaduct has an excellent database of thermocouple readings.

A concrete topping 2 in. (50 mm) thick was placed on the instrumented sections on October 7, 1996. (Note that asphalt topping was not used on this project and consequently the effects of asphalt cannot be discussed in this paper.) The net effect of placing the concrete topping on the instrumented sections is to add three additional thermocouple readings at the top, middle and bottom of the overlay and shift the remainder of the gauge

readings down by 2 in. (50 mm). This increases the overall number of gauges near the deck surface where gauge readings are desirable.

Instrumentation Results

There is an extremely large amount of data that has to be interpreted in an efficient manner in order to obtain critical positive and negative thermal gradients because the thermocouple
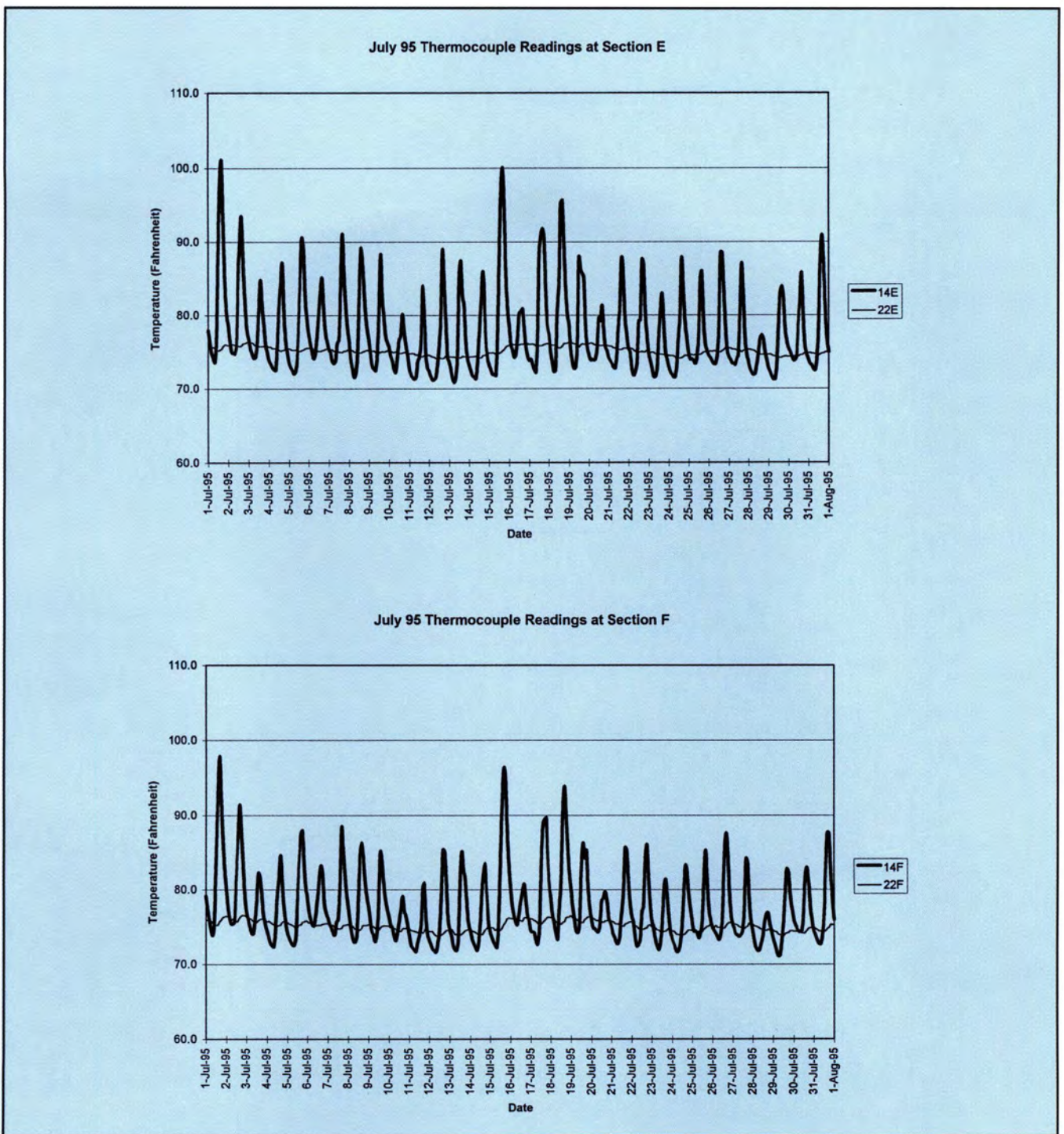
Fig. 9. July 1995 thermocouple readings.

readings are taken every 2 hours for a 5-year period at 58 gauges. (Section E has 26 gauges while Section F has 32 gauges.) The method used to reduce the data has been to graphically review the thermocouple readings on: (1) a year-by-year basis; (2) a month-by-month basis; (3) a day-by-day basis (for critical days); and, (4) a gradient-by-gradient basis (at critical times for critical days). Numerous plots of annual, monthly, daily and critical ther-

mal gradients (positive and negative) are given in Ref. 14 and only representative plots will be discussed here.

Annual readings for 1995 (see Fig. 7) and 1996 (see Fig. 8) are reviewed at Gauge 14 [2.5 in. (63 mm) below the deck surface] for Section E [8 ft (2.4 m) depth] and Section F [18 ft (5.5 m) depth]. This gives the overall picture of the thermocouple readings and what the relative high and low temperatures are in various months.

This also helps to spot spurious results (moisture in the datalogger) and no results (power failure). For instance, January 1996 readings at Section F are neglected because there was moisture in the datalogger.

Note that Gauge 14 is plotted because Gauge 13 (at the deck surface) is not reliable. Examination of Fig. 7 reveals that July 1995 appears to have some very high temperatures. Note that the peak readings at Gauge 14
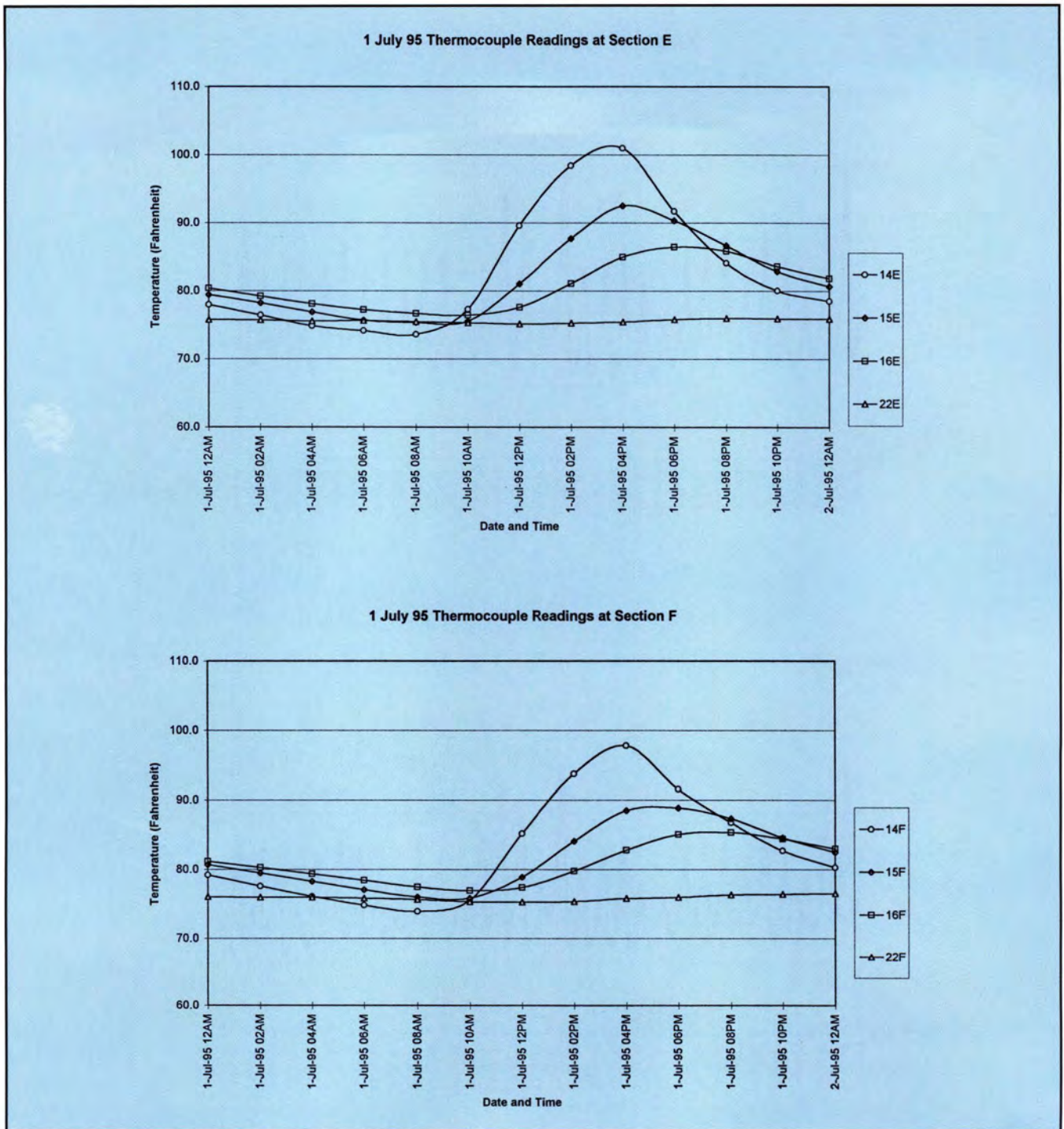
Fig. 10. July 1, 1995, thermocouple readings.

drop after August 22, 1995, due to the fact that the readings were changed from 2-hour intervals to 6-hour intervals. Furthermore, note that the peak readings at Gauge 14 drop even more after October 7, 1996, because the concrete topping has been added and Gauge 14 is now reading a value 2 in. (50 mm) lower on the thermal gradient.

Monthly readings (see Fig. 9) are reviewed at Gauge 14 and at Gauge 22.

Gauge 14 is near the deck surface and gives daily peaks and valleys. Gauge 22 is near the middle of the section and is less influenced by daily fluctuations. In general, large thermal gradients occur when the difference (positive or negative) between readings at Gauges 14 and 22 is maximum. Inspection of Fig. 9 indicates that July 1, 15 and 18 should have the largest positive thermal gradients. It is interesting to note that the readings for these days

are slightly lower for Section F than for Section E. This is because Section F [18 ft (5.5 m) depth] has a higher thermal inertia than Section E [8 ft (2.4 m) depth].

Daily readings (see Fig. 10) are reviewed at several gauges for July 1, 1995 (which has the highest July reading). Readings are plotted every 2 hours for Gauges 14, 15 and 16, which have respective distances from the deck of 2.5, 5.0 and 7.5 in. (63, 126 and 189

1-Jul-95 04PM Positive Thermal Gradient at Section E

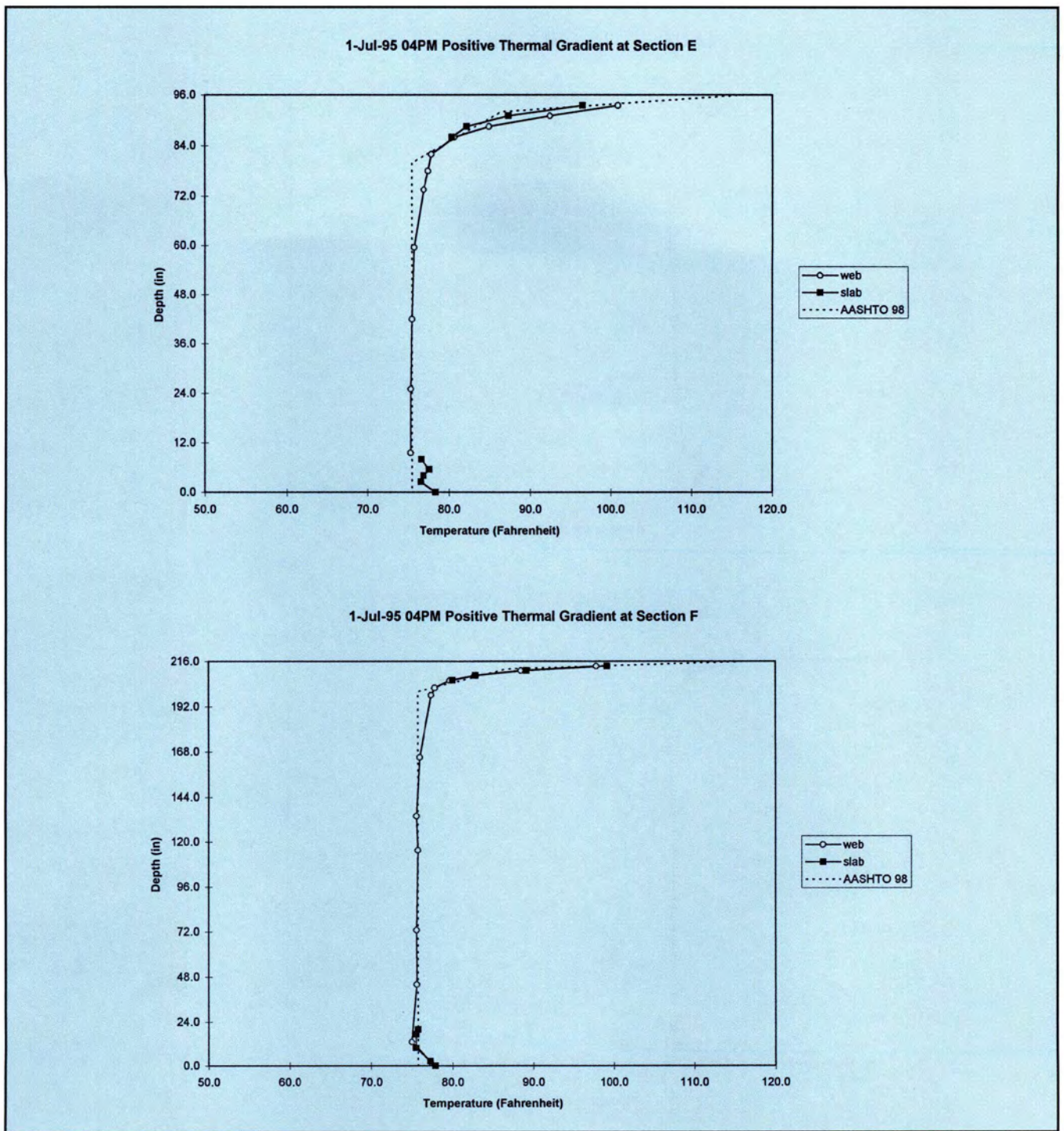**1-Jul-95 04PM Positive Thermal Gradient at Section F**

Fig. 11. July 1, 1995, positive thermal gradients.

mm) as well as Gauge 22, which is in the middle of the section. It can be seen that the maximum positive thermal gradient occurs at 4 p.m. and the maximum negative thermal gradient occurs at 8 a.m. Again, note that the maximum positive thermal gradient appears to be slightly lower for Section F than for Section E (because Section F has a higher thermal inertia than Section E).

The critical positive thermal gradients (see Fig. 11) are reviewed at 4 p.m. on July 1, 1995. Readings are plotted for gauges along the centerline of the web as well as along the centerline of the top and bottom slab. These readings are compared to those in the 1998 proposed second edition of the AASHTO segmental guide specifications (AASHTO 98). Similarly, the critical negative thermal gradients (see Fig. 12) are reviewed at 6 a.m. on May 7, 1995.

It is interesting to note that both the web and top slab values are quite close to the design gradient at both Section E and Section F. For the positive and negative thermal gradient, top slab readings are very close to the design gradient, while web readings deviate slightly from the design gradient. However, because there is much more slab area at the deck level than web area, it is very encouraging that the slab values are so close to the proposed design gradient. These values and others in the report[14] should help

7-May-95 06AM Negative Thermal Gradient at Section E

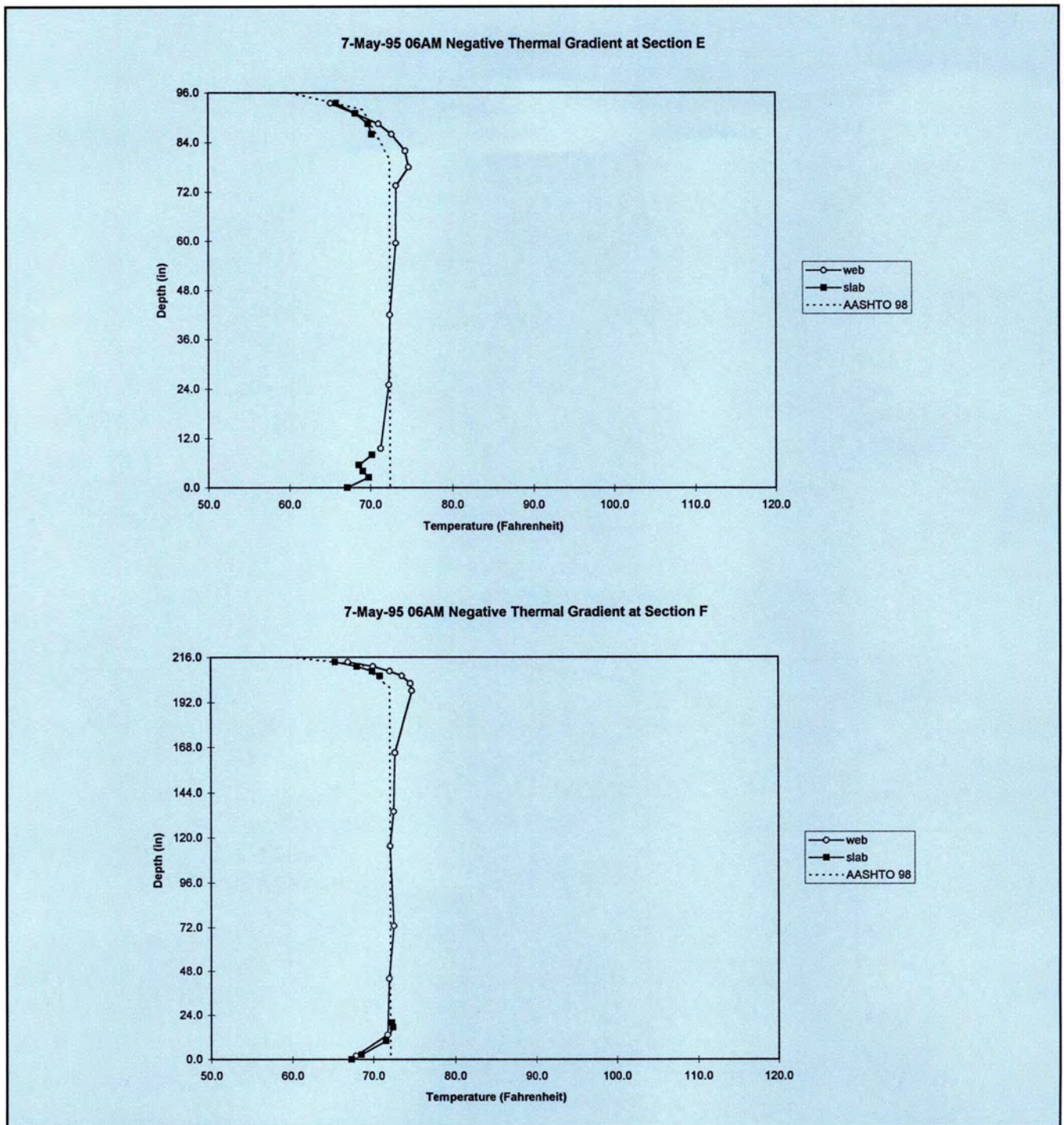**7-May-95 06AM Negative Thermal Gradient at Section F**

Fig. 12. May 7, 1995, negative thermal gradients.

to validate the use of this proposed design gradient.

Extrapolation should be used to determine the temperatures at the deck level (because readings for Gauge 13 are unreliable). At Section F, the positive and negative thermal gradient both show a peak at the bottom of the section; the web and bottom slab values are quite close to each other. At Section E, the peak at the bottom is less clearly defined; the bottom slab value

is jagged (and there is no gauge in the web at the bottom). The proposed design gradients (AASHTO 98) also indicate that peaks at the bottom will occur but that they can be neglected.

ANALYSIS OF NORTH HALAWA VALLEY VIADUCT

Analysis for Thermal Gradient

In general, thermal stresses are induced by restraint to expansion and

rotation, and not by temperature changes directly. Restraint is provided by the cross section and the support conditions. The cross section induces primary stresses that vary in the vertical direction but are constant in the longitudinal direction (if the section is constant). The support conditions induce secondary stresses that vary in the longitudinal direction.

For a positive thermal gradient (see Fig. 13), the compressive thermal

stress component can be considered as being equilibrated by a tensile resultant force P at some distance e_{top} from the top of the section. This resultant force is equivalent to a tensile axial force N_p and a negative bending moment M_p at the location of the neutral axis y_{top} from the top of the section.

The primary stress (see Fig. 14) is the superposition of the thermal component $f(y)$ with the axial component N_p/A and the flexural component $M_p y/I$. The support conditions cause redistribution to occur and create compressive axial forces N_s and positive bending moments M_s. The secondary stress (see Fig. 14) is the superposition of the axial component N_s/A and the flexural component $M_s y/I$. The total stress is the superposition of the primary and secondary stresses (see Fig. 14). (For more details see Refs. 7 and 8.)

The calculations can be simplified substantially by recognizing that the resultant axial force P and location from the top e_{top} due to the thermal component are constant for segmental bridges (see Fig. 13). This is due to the fact that the dimensions at the top of a segmental bridge are normally constant and the thermal gradient acts near the top of the section. The net result is that once P and e_{top} have been determined for one section, the pri-
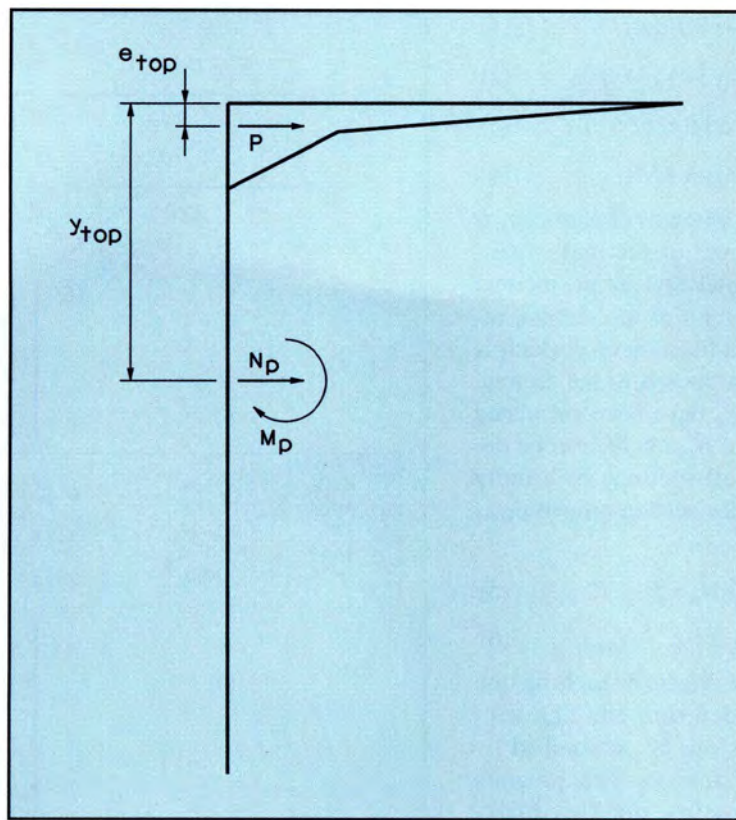
mary and secondary effects at any section can be found by a simple manipulation of the section properties.

On the other hand, if the effects of the thermal component are taken about the neutral axis or the bottom of the section (as has commonly been done in the past), a completely new set of

calculations has to be made at each location because the depth of the section and/or bottom slab thickness are normally variable.

Expressions for the thermal component $f(y)$, axial force P, bending moment about the top M and eccentricity about the top e_{top} are given as follows:

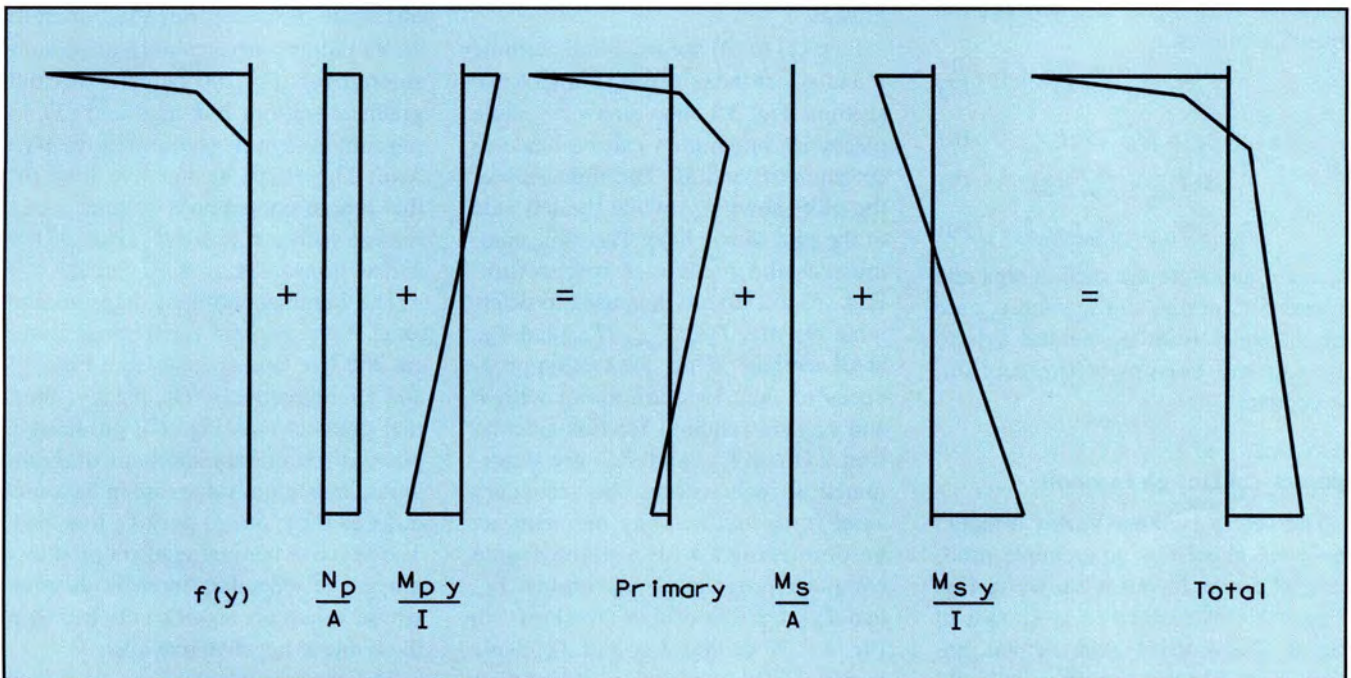Fig. 13. Positive thermal gradient and equivalent forces.

Fig. 14. Stresses due to positive thermal gradient.

$$f(y) = E\alpha t(y) \qquad (1)$$

$$P = E\alpha \int t(y)\, b(y)\, dy \qquad (2)$$

$$M = E\alpha \int t(y)\, b(y)\, y\, dy \qquad (3)$$

$$e_{top} = M/P \qquad (4)$$

where E is the modulus of elasticity, α is the coefficient of thermal expansion, and $t(y)$ and $b(y)$ are the thermal gradient and width of the section, respectively, as a function of y which is measured from the top of the section. Once P and e_{top} have been calculated for one section, N_p and M_p can be determined for all sections by simply working with the section properties as follows:

$$N_p = P \qquad (5)$$

$$M_p = P(y_{top} - e_{top}) \qquad (6)$$

The primary effects at each section can now be determined. The secondary effects can be determined by using a plane frame computer program (or by hand using the flexibility method). Three methods can be used to input thermal data into a plane frame computer program:

1. Axial force and bending moment (N_p and M_p).

2. Equivalent uniform temperature and linear gradient (T_{unif} and T_{grad}).

3. Temperature at the top and bottom of the section (T_{top} and T_{bot}).

The method chosen depends on the capabilities of the program. Expressions for T_{unif}, T_{grad}, T_{top} and T_{bot} are given as follows:

$$T_{unif} = N_p/(E\alpha A) \qquad (7)$$

$$T_{grad} = M_p/(E\alpha I) \qquad (8)$$

$$T_{top} = T_{unif} + T_{grad} y_{top} \qquad (9)$$

$$T_{bot} = T_{unif} - T_{grad} y_{bot} \qquad (10)$$

where A and I are the section area and moment of inertia, and y_{top} and y_{bot} are the distances from the neutral axis to the top and bottom of the section, respectively.

Numerical Design Example

The North Halawa Valley Viaduct has been chosen as an example problem. The span layout is shown in Fig. 5 and the cross section is shown in Fig. 4. The AASHTO 98 thermal gradient is used in this example. It should be emphasized again that the methods
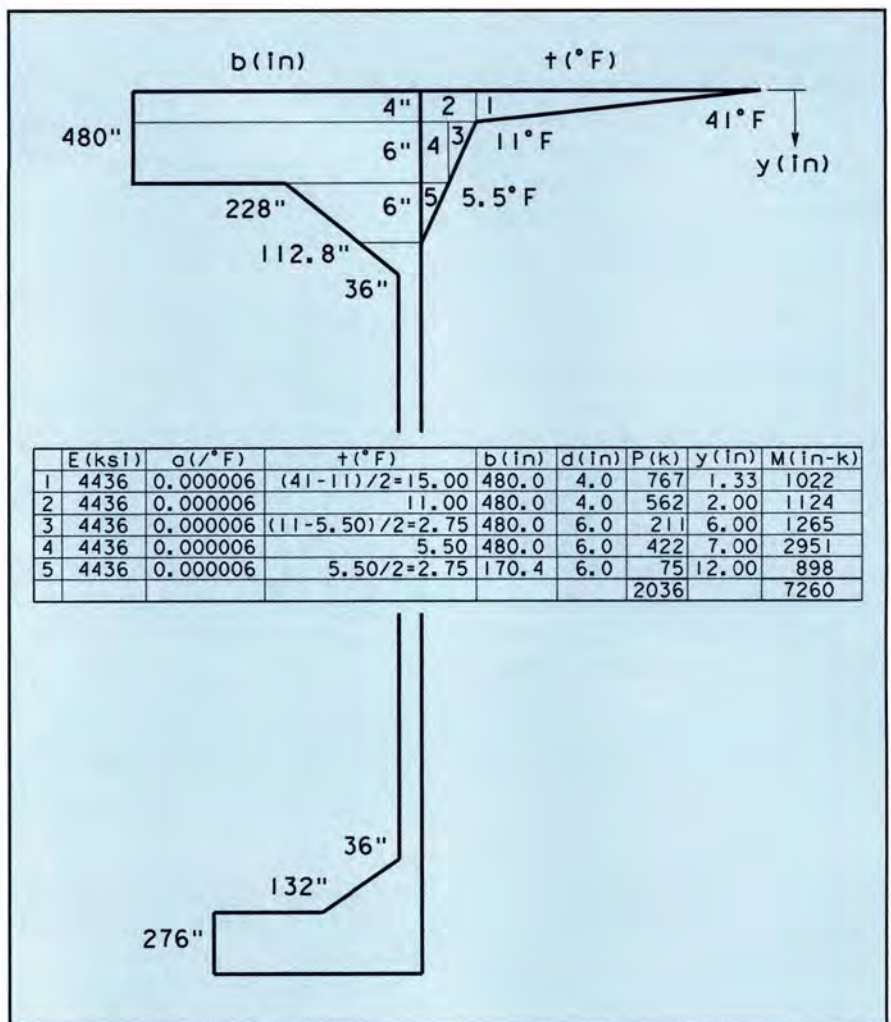

Fig. 15. Calculation of P and M.

	E(ksi)	α(/°F)	t(°F)	b(in)	d(in)	P(k)	y(in)	M(in-k)
1	4436	0.000006	(41-11)/2=15.00	480.0	4.0	767	1.33	1022
2	4436	0.000006	11.00	480.0	4.0	562	2.00	1124
3	4436	0.000006	(11-5.50)/2=2.75	480.0	6.0	211	6.00	1265
4	4436	0.000006	5.50	480.0	6.0	422	7.00	2951
5	4436	0.000006	5.50/2=2.75	170.4	6.0	75	12.00	898
						2036		7260

given in this paper apply equally to precast and cast-in-place segmental bridges.

Eqs. (1) to (4) are used to determine P and e_{top} at the midspan [8 ft (2.4 m)] section. Fig. 15 shows how a simple piecewise integration can be made to determine P and M. The right side of the plot shows $t(y)$ while the left side of the plot shows $b(y)$. The table summarizes the piecewise integration. Eqs. (5) to (10) are then used to determine N_p, M_p, T_{unif}, T_{grad}, T_{top} and T_{bot} at all sections. (Only the section properties at each location along with P and e_{top} are required for this calculation.) Once T_{top} and T_{bot} are determined at each section, the secondary axial force and bending moment can be determined with a plane frame computer program. Temperatures T_{top} and T_{bot} for this bridge are shown in Fig. 16. Note that T_{top} and T_{bot} have larger values at midspan and smaller values at the support.

For the remainder of this study, it is worthwhile to compare thermal gradient with live load because current codes require serviceability to be considered for: (1) 100 percent thermal gradient without live load and (2) 50 percent thermal gradient with live load. The HS20 design live load for this bridge corresponds to three lanes loaded with a reduction factor of 0.9 and an impact factor of 10 percent.

The bending moment diagram and axial force diagram for thermal gradient and live load are shown in Figs. 17 and 18, respectively. The positive thermal gradient (see Fig. 17) produces a positive secondary moment diagram whose maximum values are in the same order as those due to positive live load. The negative thermal gradient produces a negative secondary moment diagram whose values are significantly less than those due to negative live load.

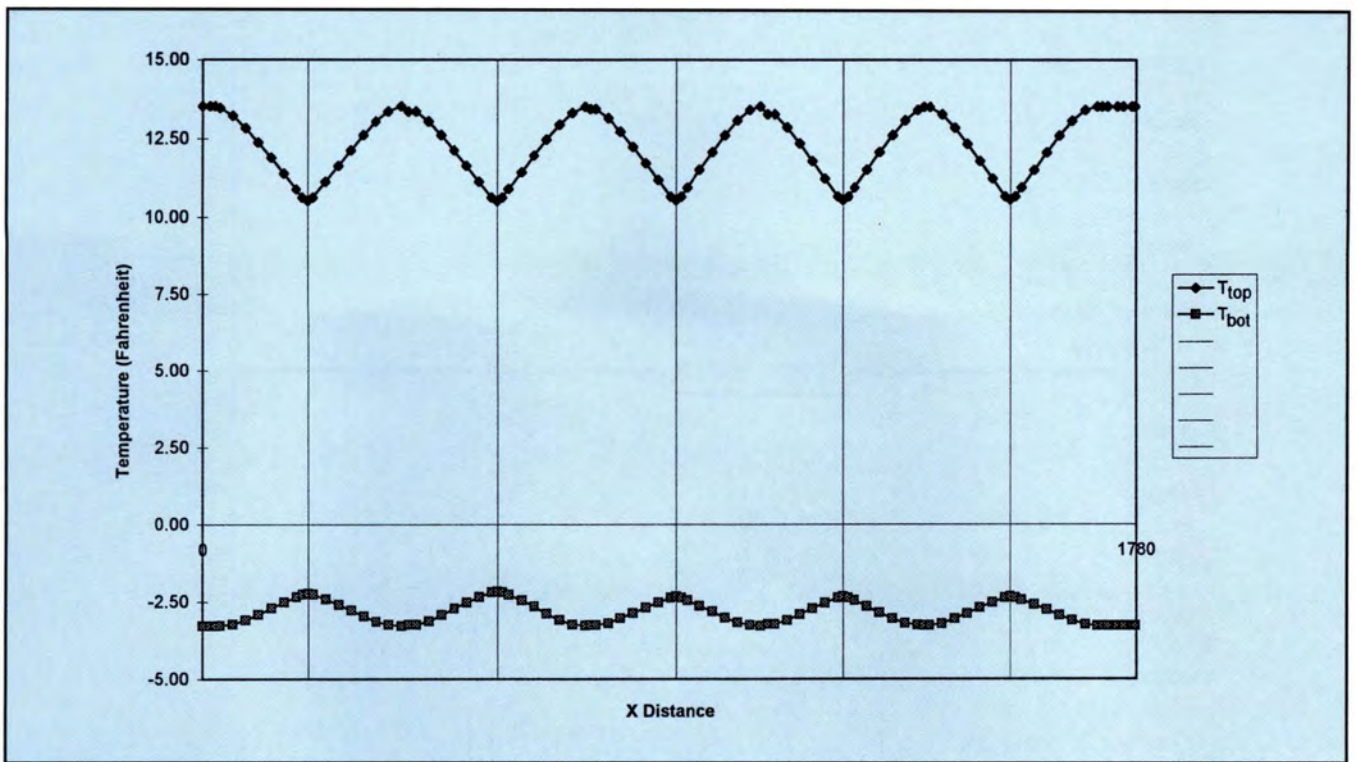The positive thermal gradient (see Fig. 18) produces a uniform com-

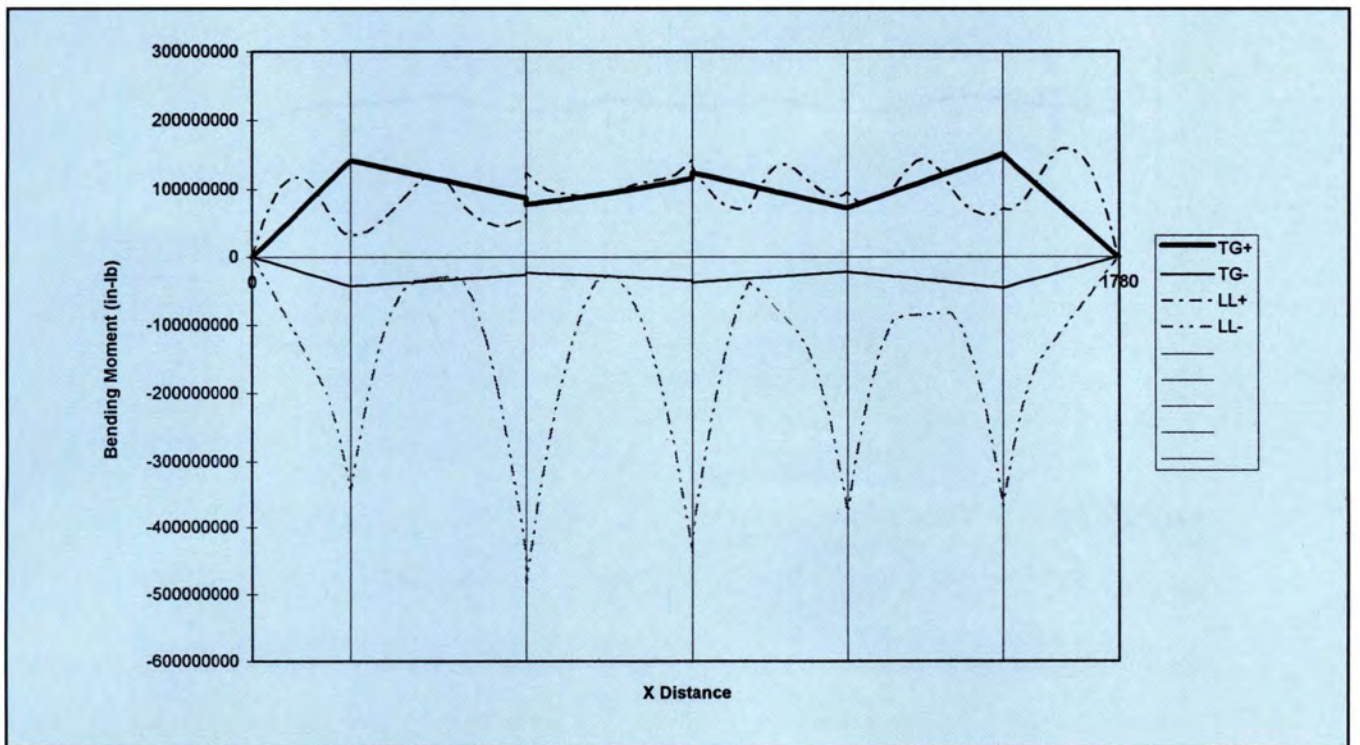Fig. 16. Temperatures for equivalent linear thermal gradient.

Fig. 17. Bending moment diagram for thermal gradient and live load.

pressive axial force in Span 9-10, which has fixed piers at both ends. The corresponding variable compressive axial force due to positive live load is also shown. The negative thermal gradient and negative live load, respectively, produce a uniform and variable tensile axial force in Span 9-10.

The stresses at the top and bottom of the section due to thermal gradient and live load are shown in Figs. 19 and 20, respectively. Tensile stresses are of primary importance here because additional prestressing is required to keep values within allowable limits; compressive stresses are also of interest but normally not a problem because there is usually a sufficient reserve of compression.

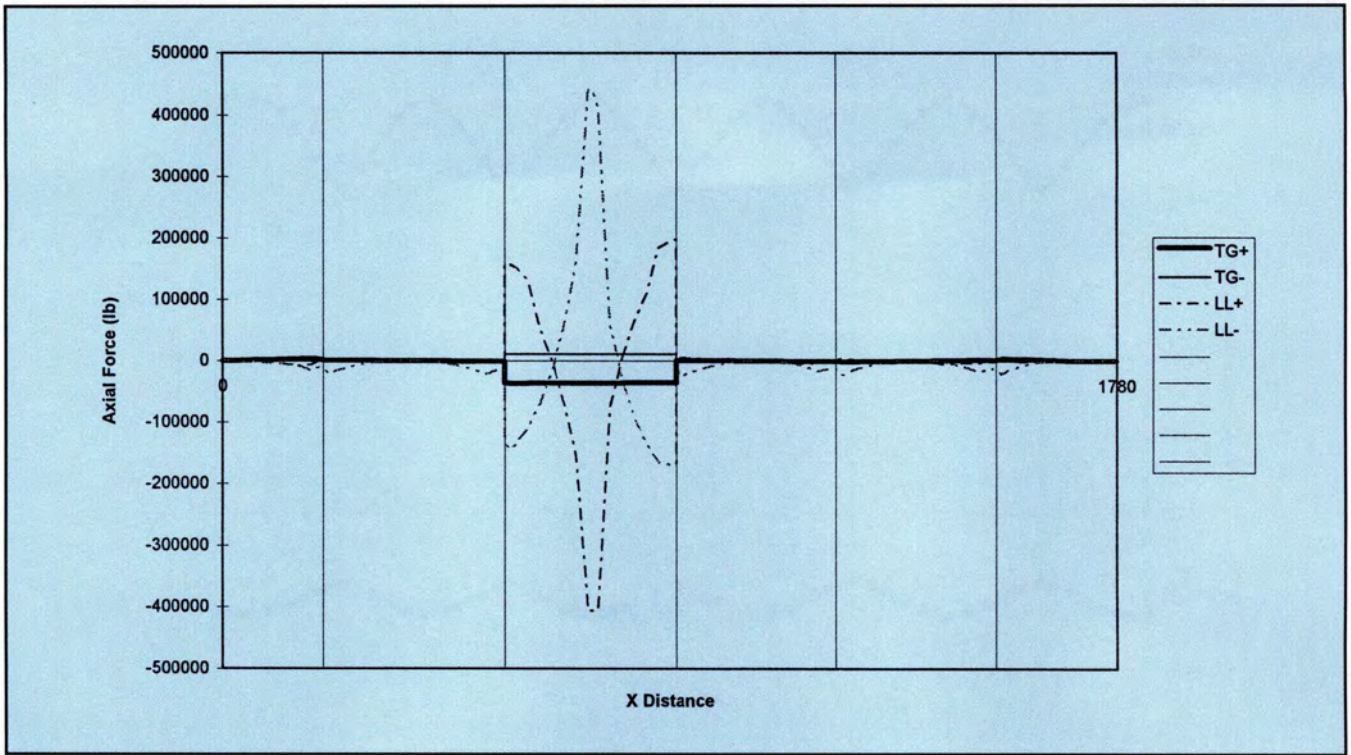The negative thermal gradient (see Fig. 19) causes approximately uniform

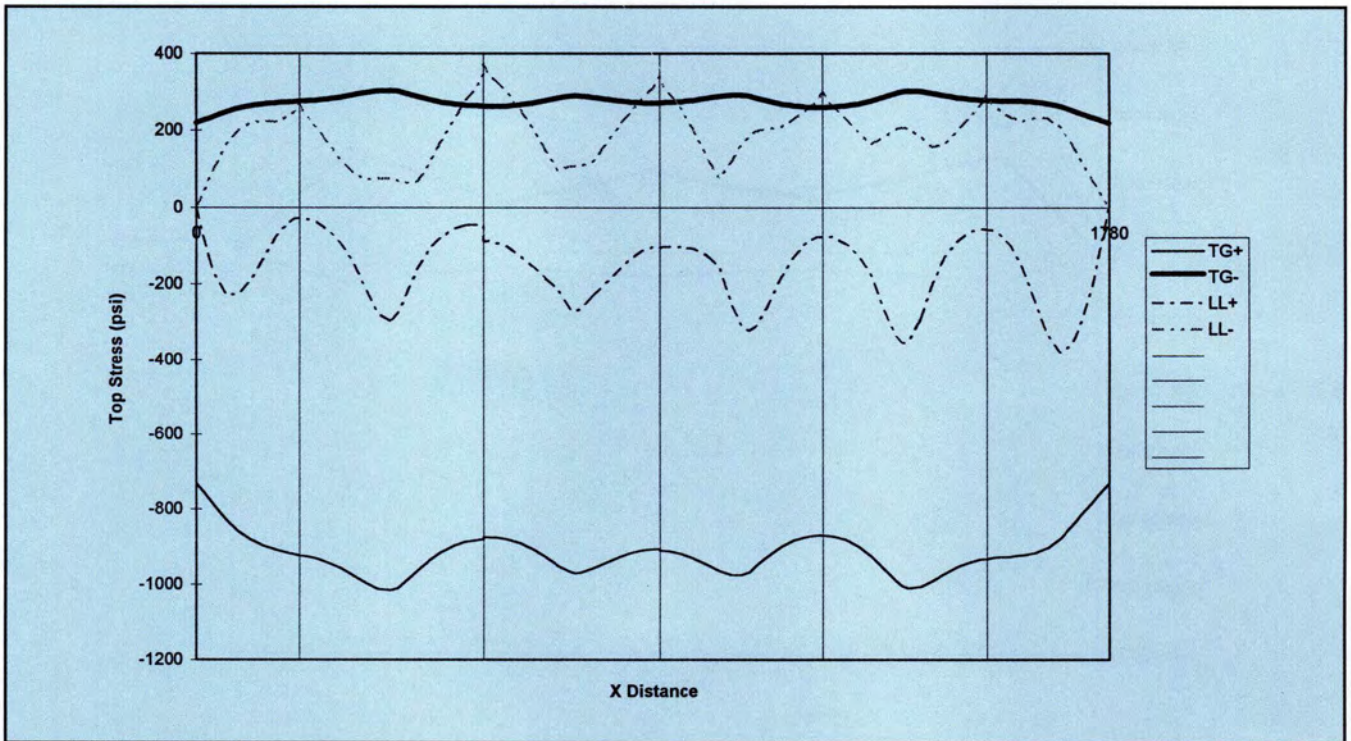Fig. 18. Axial force diagram for thermal gradient and live load.

Fig. 19. Top stress diagram for thermal gradient and live load.

tension to occur at the top. The amount of tension varies from a minimum of 220 psi (1.52 MPa) at the ends of the bridge to a maximum of 305 psi (2.10 MPa) at midspan of Span 8-9 [360 ft (110 m) span]. The amount of prestressing (top continuity

tendons) may have to be increased at midspan to accommodate this tension.

Both positive thermal gradient (see Fig. 20) and positive live load cause variable tension at the bottom, which is maximum at midspan. For the four interior spans, the ratio of thermal gra-

dient stress to live load stress is 78 percent for Span 8-9, 84 percent for Span 9-10, 60 percent for Span 10-11 and 64 percent for Span 11-12. Thus, the stress due to thermal gradient can be of the same order (60 to 80 percent) as that due to live load. The amount of
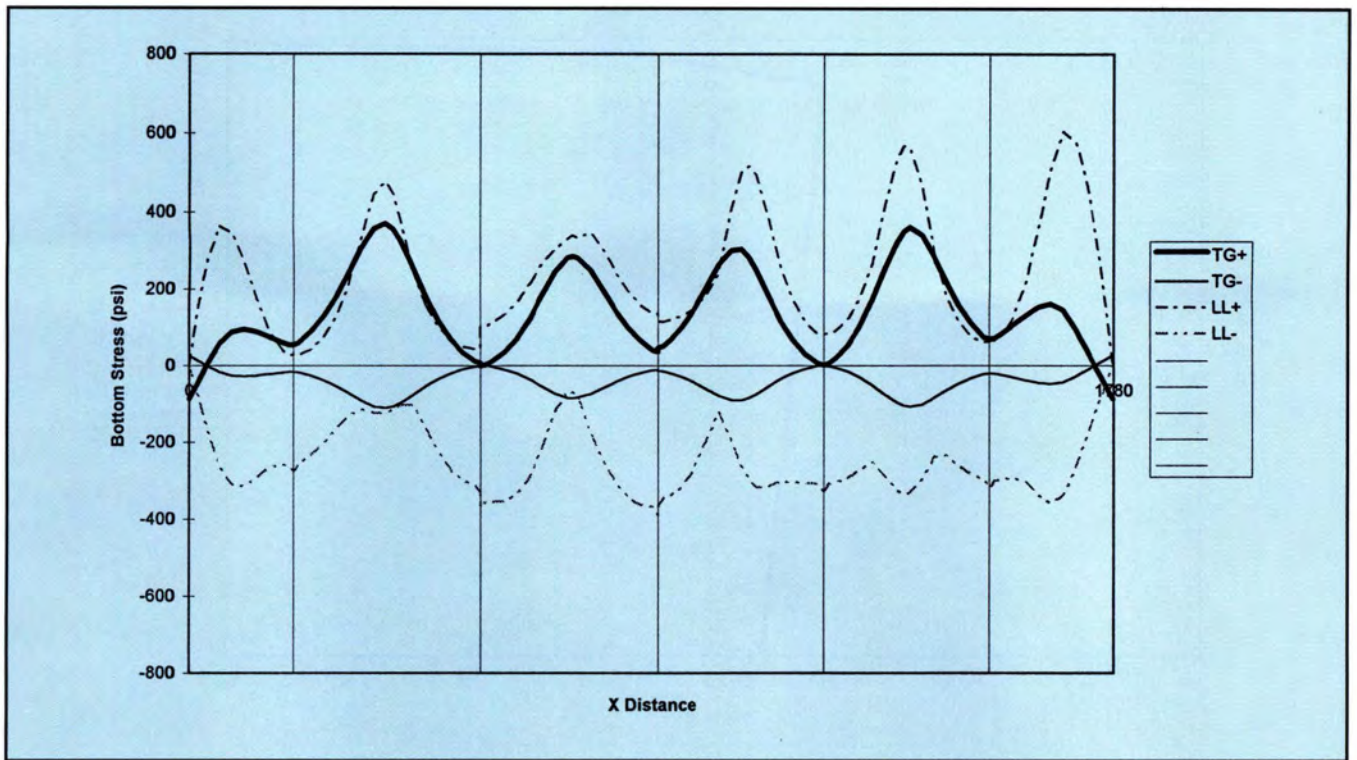
Fig. 20. Bottom stress diagram for thermal gradient and live load.
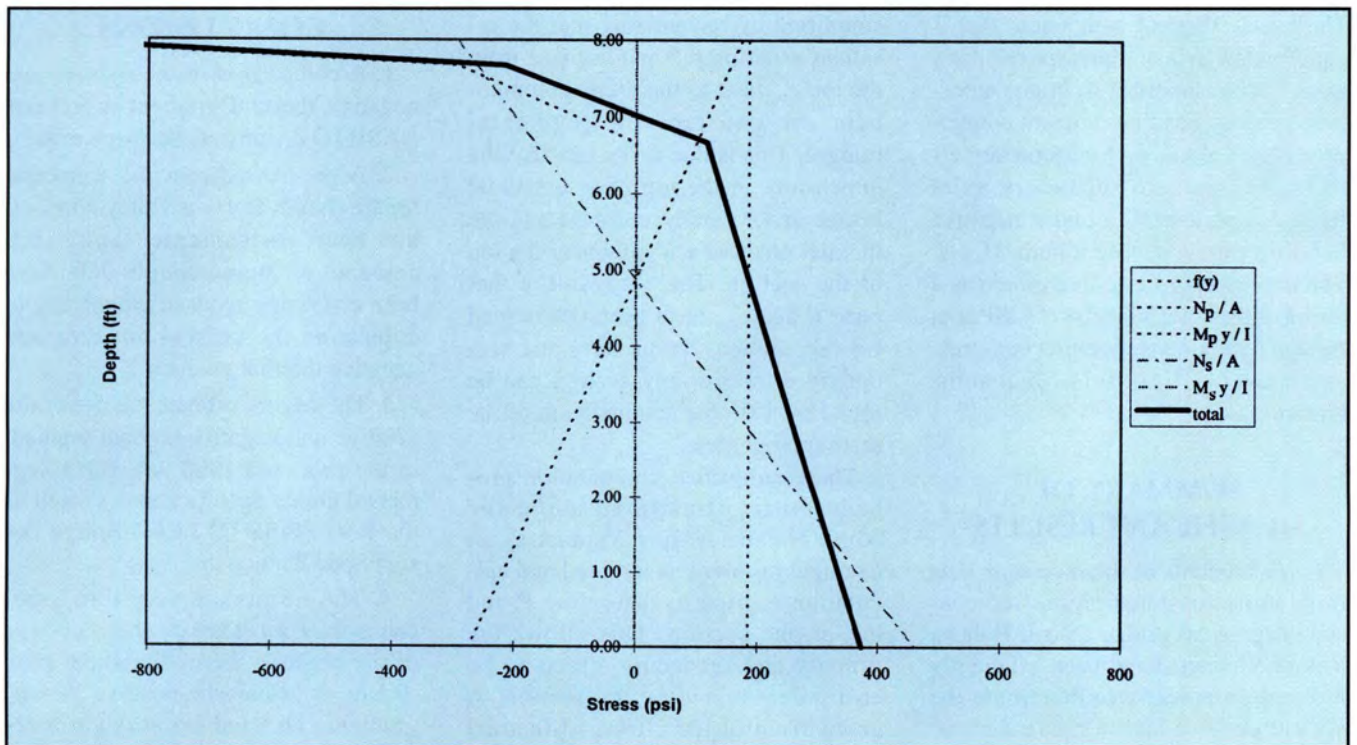

Fig. 21. Thermal stresses at midspan of Span 8-9 for positive thermal gradient.

prestressing (bottom continuity tendons) has to be increased to accommodate the case of live load plus 50 percent thermal gradient.

Thermal stresses at midspan of Span 8-9 [360 ft span (110 m)] for a positive gradient are shown in Fig. 21. The compressive thermal component $f(y)$ is equilibrated by a tensile primary axial force component N_p/A and a negative primary bending moment component $M_p y/I$. Analysis for secondary effects gives a zero secondary axial force component N_s/A and a positive bending moment component $M_s y/I$. The net result of these five effects is a tensile stress of 374 psi (2.58 MPa) at the bottom with a corresponding compressive stress of 1026 psi (7.07 MPa) at the top.

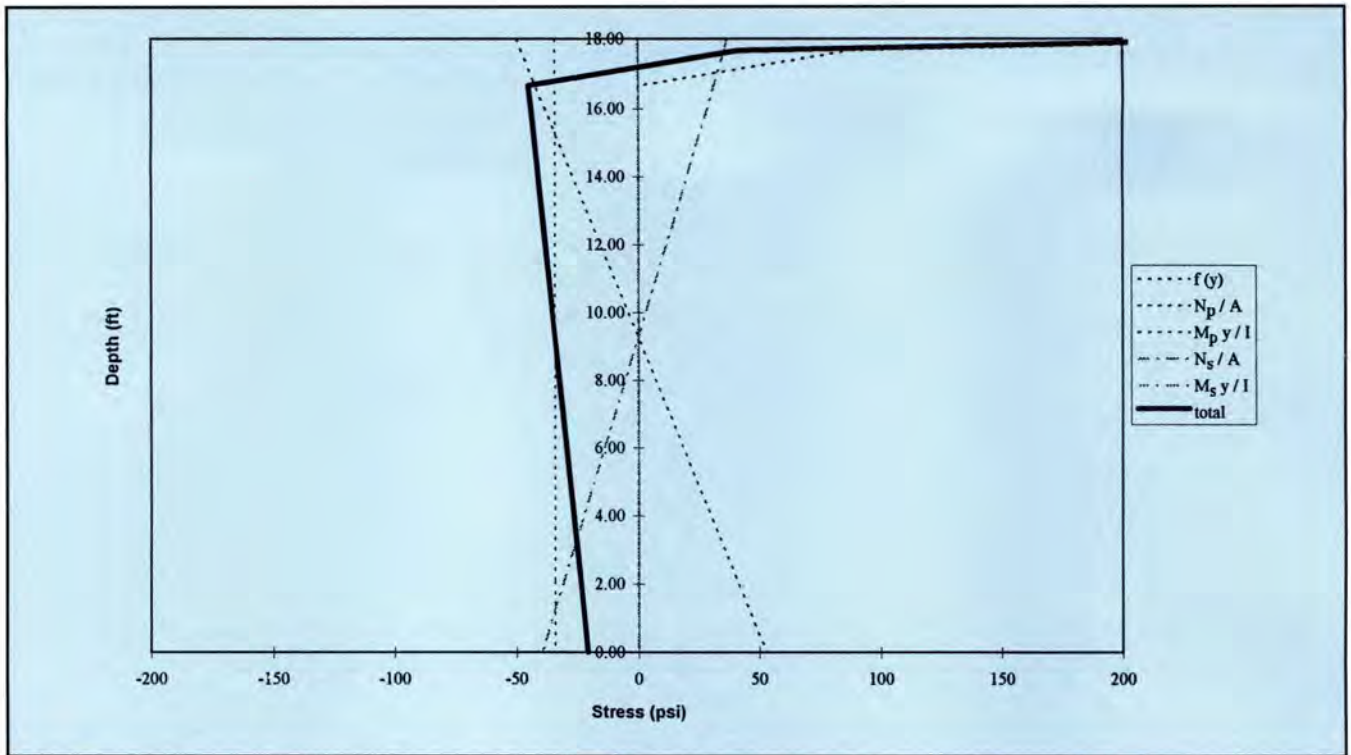Thermal stresses at Pier 12 for a negative gradient are shown in Fig. 22.

Fig. 22. Thermal stresses at Pier 12 for negative thermal gradient.

The tensile thermal component $f(y)$ is equilibrated by a compressive primary axial force component N_p/A and a positive primary bending moment component $M_p y/I$. Analysis for secondary effects gives a zero secondary axial force component N_s/A and a negative bending moment component $M_s y/I$. The net result of these five effects is a tensile stress of 280 psi (1.93 MPa) at the top with a corresponding compressive stress of 21 psi (0.14 MPa) at the bottom.

SUMMARY OF SIGNIFICANT RESULTS

Large amounts of thermocouple data from an instrumented prestressed concrete segmental bridge (North Halawa Valley Viaduct) have been efficiently reduced graphically to determine the critical positive and negative thermal gradients. The results validate the use of the positive and negative thermal gradient in the proposed 1998 AASHTO Segmental Guide Specifications (which is similar for positive gradient and reduced by 40 percent for negative gradient from the 1994 AASHTO LRFD Bridge Design Specifications).

The computation procedures for a nonlinear thermal gradient are greatly

simplified by recognizing that the resultant axial force P and distance from the top e_{top} due to the thermal component are constant for segmental bridges. This is due to the fact that the dimensions at the top of a segmental bridge are normally constant and the thermal gradient acts only near the top of the section. The net result is that once P and e_{top} have been determined for one section, the primary and secondary effects at any section can be found by a simple manipulation of the section properties.

These simplified computation procedures are illustrated using the North Halawa Valley Viaduct as an example problem. A simple hand calculation is used to determine P and e_{top} at one section. This allows the primary and secondary effects to be easily determined at any section. A comparison of the effects of thermal gradient and live load is made with respect to the prestressing requirements. Additional prestressing is required at the bottom near midspan for the case of live load plus 50 percent positive thermal gradient. Additional prestressing may also be required at the top near midspan to accommodate the negative thermal gradient.

CONCLUSIONS

1. A comparison of the positive and negative thermal gradient in various AASHTO documents has been made.

2. A prestressed concrete segmental bridge (North Halawa Valley Viaduct) has been instrumented and large amounts of thermocouple data have been efficiently reduced graphically to determine the critical positive and negative thermal gradient.

3. The results validate the use of the positive and negative thermal gradient in the proposed 1998 AASHTO Segmental Guide Specifications as well as the 1994 AASHTO LRFD Bridge Design Specifications.

4. The results are very timely because they substantiate the reduction of the negative thermal gradient from -0.5 to -0.3 times the positive thermal gradient. This reduction is currently being considered in the proposed 1998 AASHTO Segmental Guide Specifications.

5. The computation procedures for nonlinear thermal gradient have been shown to be greatly simplified by recognizing that the resultant axial force P and location from the top e_{top} due to the thermal component are constant for most segmental bridges. Once P and

e_{top} have been determined for one section, the primary and secondary effects at any section can be found by a simple manipulation of the section properties.

6. A numerical example for the analysis of a segmental bridge for thermal gradient has been included. A simple hand calculation is used to determine P and e_{top} at one section. This allows the primary and secondary effects to be determined at all sections.

7. The numerical example includes a comparison of forces and stresses due to thermal gradient and live load. This allows a comparison of the prestressing requirements. Additional prestressing is required at the bottom near midspan for the case of live load plus 50 percent positive thermal gradient. Additional prestressing may also be required at the top near midspan to accommodate the negative thermal gradient.

REFERENCES

1. *Precast Segmental Box Girder Bridge Manual*, Published jointly by the Prestressed Concrete Institute, Chicago, Illinois, and Post-Tensioning Institute, Phoenix, AZ, 1978, pp. 41-44.
2. Priestley, M. J. N., "Design of Concrete Bridges for Temperature Gradients," *ACI Journal*, V. 75, No. 5, May 1978, pp. 209-217.
3. Hoffman, P. C., McClure, R. M., and West, H. H., "Temperature Study of an Experimental Segmental Bridge," PCI JOURNAL, V. 28, No. 2, March-April 1983, pp. 78-97.
4. Elbadry, M. M., and Ghali, A., "Temperature Variations in Concrete Bridges," *Journal of Structural Engineering*, V. 20, No. 10, October 1983, pp. 2355-2374.
5. Cooke, N., Priestley, M. J. N., and Thurston, S. J., "Analysis and Design of Partially Prestressed Concrete Bridges Under Thermal Loading," PCI JOURNAL, V. 29, No. 3, May-June 1984, pp. 94-115.
6. Potgieter, I. C., and Gamble, W. L., "Nonlinear Temperature Distributions in Bridges at Different Locations in the United States," PCI JOURNAL, V. 34, No. 4, July-August 1989, pp. 80-103.
7. Imbsen, R. A., Vandershaf, D. E., Schamber, R. A., and Nutt R. V., "Thermal Effects in Concrete Bridge Superstructures," National Cooperative Highway Research Program Report 276, Transportation Research Board, Washington, D.C., September 1985, 99 pp.
8. AASHTO, *Guide Specifications — Thermal Effects in Concrete Bridge Superstructures*, First Edition, American Association of State Highway and Transportation Officials, Washington, D.C., 1989.
9. AASHTO, *Guide Specifications for Design and Construction of Segmental Concrete Bridges*, First Edition, American Association of State Highway and Transportation Officials, Washington, D.C., 1989.
10. AASHTO, *LRFD Bridge Design Specifications*, First Edition, American Association of State Highway and Transportation Officials, Washington, D.C., 1994.
11. AASHTO, *Guide Specifications for Design and Construction of Segmental Concrete Bridges*, Proposed Second Edition, American Association of State Highway and Transportation Officials, Washington, D.C., 1998.
12. Ingham, T. J., Manzanarez, R., and Cormier, K., "Design and Construction of North Halawa Valley Viaduct," Proceedings of Fourth International Bridge Engineering Conference, San Francisco, CA, 1995, pp. 176-184.
13. Lee, A., and Robertson, I. N., "Instrumentation and Long-Term Monitoring of the North Halawa Valley Viaduct," University of Hawaii at Manoa, Department of Civil Engineering Report UHM/CE/95-08, 1995.
14. Shushkewich, K. W., Vo, N. T., and Robertson, I. N., "Instrumentation of the North Halawa Valley Viaduct — Oahu, Hawaii," Progress Report to Hawaii Department of Transportation and Federal Highway Administration, 1998.

APPENDIX — NOTATION

α = coefficient of thermal expansion
A = section area
$b(y)$ = width of section as a function of y
E = modulus of elasticity
e_{top} = eccentricity of thermal stress component about top
$f(y)$ = thermal stress component as a function of y
I = section moment of inertia
M = bending moment resisting thermal stress component
M_p = primary bending moment
M_s = secondary bending moment
N_p = primary axial force

N_s = secondary axial force
P = axial force resisting thermal stress component
T_{bot} = temperature at bottom of section
T_{grad} = linear gradient
T_{top} = temperature at top of section
T_{unif} = uniform temperature
$t(y)$ = thermal gradient as a function of y
y = distance measured from top of section
y_{bot} = distance from neutral axis to bottom of section
y_{top} = distance from neutral axis to top of section